Quantum effects in the dynamics of He probed by inelastic x-ray scattering

R. Verbeni,[1] A. Cunsolo,[2] G. Pratesi,[3] G. Monaco,[1] F. Rosica,[4] C. Masciovecchio,[5] M. Nardone,[2] G. Ruocco,[4] F. Sette,[1] and F. Albergamo[5]

[1]*European Synchrotron Radiation Facility, Boîte Postal 220, F-38043 Grenoble Cedex, France*

[2]*Istituto Nazionale di Fisica della Materia, Università degli Studi Roma Tre, Via della Vasca Navale, 84 00146, Roma, Italy*

[3]*Istituto Nazionale di Fisica della Materia, I-50139, Firenze, Italy*

[4]*Università di Roma "La Sapienza" and INFM, I-00185, Roma, Italy*

[5]*Sincrotone Trieste, Area Science Park, I-34017, Trieste, Italy*

(Received 3 October 2000; revised manuscript received 2 April 2001; published 24 July 2001)

Quantum effects in the teraherz dynamics of supercritical ^{4}He have been studied as a function of both density ρ and temperature T; they have been characterized through their effects on the second and third spectral moments of the dynamic structure factor $S(Q,\omega)$, measured by the inelastic x-ray scattering (IXS) technique. The IXS spectra were collected in the low-Q region below and around the position of the first diffraction peak Q_m, i.e., in a range relatively unusual in this kind of investigation. The measured spectral moments clearly show a departure from their high-T classical expected values. We observe, moreover, that the amplitude of quantum deviations increases slightly with increasing density. This experimental method allows us to extract, even in a region where the dynamics still maintains a collective character, such typical single particle properties as the mean atomic kinetic energy.

DOI: 10.1103/PhysRevE.64.021203 PACS number(s): 51.10.+y, 61.10.Eq, 61.20.Ja, 78.70.Ck

I. INTRODUCTION

During the last two decades, the study of the dynamical structure factor of helium has been the focus of several experimental [1,2], computational [3,4], and theoretical [5] works. However, while the higher-(Q,ω) portion of the kinematic plane, dominated by the single particle regime, as well as the lowest-(Q,ω) portion, dominated by classical hydrodynamic behavior, have been rather thoroughly explored, no comparable effort has been addressed to the study of the intermediate-(Q,ω) region, where collective modes deeply influence the dynamics and quantum effects can no longer be neglected. The transition between classical and quantum dynamical regimes, which occurs gradually as Q is increased, is one of the main motivations for studying this dynamical region experimentally. Indeed at the lowest-(Q,ω) values, such as those usually probed by Brillouin light scattering, deviations from the classical behavior are hardly discernible since the quantum aspects of the dynamics become evident only when Q and ω become comparable with the inverse of the quantum coherence length and time, respectively, given, roughly speaking, by λ_B^{-1} and $c\lambda_B^{-1}$ (λ_B being the de Broglie wavelength and c the speed of light in vacuum). This transition is expected to occur in the range explored by high-frequency spectroscopic techniques such as inelastic neutron scattering and inelastic x-ray scattering (IXS). Since scattering techniques all probe the dynamical structure factor $S(Q,\omega)$, a straightforward quantitative method to pin down quantum effects in the collective dynamics is provided by the measurement of its second spectral moment $\langle\omega^2(Q)\rangle=\int\omega^2 S(Q,\omega)d\omega$ and, in particular, of its deviations from the high-temperature classical limit given by $(k_BT/M)Q^2$ (k_B being the Boltzmann constant and M the atomic mass).

In the present work we will characterize this transition as a function of both density ρ and temperature T in a strongly quantum fluid such as ^{4}He. This characterization will be achieved by evaluating the Q behavior of $\langle\omega^2(Q)\rangle$ obtained from the experimental $S(Q,\omega)$ measured by inelastic x-ray scattering.

We recall here that in this dynamic range the IXS technique provides a twofold advantage compared to inelastic neutron scattering, namely, (i) owing to the reduced transverse size of the beam it allows small sized samples to be probed thus allowing extreme thermodynamic conditions to be reached; (ii) the IXS cross section of He is virtually free from incoherent contributions to $S(Q,\omega)$. Unfortunately, spectral moments of any order $\langle\omega^n(Q)\rangle$ evaluated directly from IXS spectra are affected by a number of nontrivial systematic uncertainties mainly arising from the finite instrumental resolution. In order to cope with this problem, we have estimated the spectral moments of the resolution free line shapes $S(Q,\omega)$ by fitting the IXS spectra with a reliable model line shape $S_M(Q,\omega)$ and computing its spectral moments $\langle\omega_M^n(Q)\rangle$. This practice implies on one hand that one must be confident in the ability of the model to reproduce the data up to frequency values where the integrals $\int\omega^n S(Q,\omega)d\omega$ have already reached convergence and on the other hand that the data themselves are, in the same frequency range, of sufficient statistical accuracy to allow a significant fit procedure. Since the model line shape adopted has a limited number of converging moments, we are able to compute in principle only the first four spectral moments $(n=0,1,2,3)$. Furthermore, in order to overcome intensity normalization problems, we will normalize the data to the first moment $\langle\omega^1(Q)\rangle$, the expected value of which is exactly known. We will therefore deal essentially with the two independent moment ratios R_n (with $n=2$ or 3) given by

$$R_n=\frac{\hbar^n\langle\omega^n(Q)\rangle}{\hbar\langle\omega^1(Q)\rangle}, \tag{1}$$

which, exploiting the well known first moment sum rule [12], can also be written as

$$R_n = \hbar^{(n-2)} \frac{2M\langle \omega^n(Q) \rangle}{Q^2}. \tag{2}$$

It is worthwhile noticing that the zeroth moment ratio can in principle be exploited to yield the structure factor $S(Q)$ of the fluid,

$$R_0 = \frac{\langle \omega^0(Q) \rangle}{\hbar \langle \omega^1(Q) \rangle} = \frac{2M\langle \omega^0(Q) \rangle}{\hbar^2 Q^2} = \frac{2MS(Q)}{\hbar^2 Q^2}. \tag{3}$$

II. THE EXPERIMENT

The experiment was carried out at the very high-energy-resolution IXS beamline (ID16) at the European Synchrotron Radiation Facility. The spectrometer consists of a backscattering monochromator and five independent analyzers, mounted on the tip of a 7 m long arm and set next to each other with a constant angular offset. The experimental assembly, based on high-order reflections from silicon single crystals in backscattering geometry, was used at the Si(9,9,9) reflection with incident energy of 17.494 keV. The resolution function, determined experimentally by measuring the spectral density scattered by a Plexiglass sample around the first diffraction peak ($Q=10$ nm^{-1}), has a full width at half maximum of 3.5 ± 0.1 meV for each of the five analyzers. The spectrometer arm can be rotated in the horizontal plane, in order to select the exchanged momentum [$Q=(4\pi/\lambda)\sin\vartheta/2$]. The Q resolution was set to ± 0.2 nm^{-1}. In the present IXS experiment the Q values ranged between 2.5 and 25.9 nm^{-1}, thus ranging up to the first maximum of $S(Q)$ ($Q_m \sim 24.5$ nm^{-1}), while the frequencies $\omega/2\pi$ are in the THz range.

Further details of the beamline are reported elsewhere [6].

The sample was contained in a valve sealed two-window steel cell kept, under vacuum, in thermal contact with a closed cycle refrigerator head. The incident and essentially forward scattered x-ray beams enter and leave the sample through two cylindrical single crystal diamond windows (thickness 1 mm; diameter 2.3 mm). The distance between the two windows, i.e., the sample length along the beam, is 20 mm, roughly one-tenth of the photoelectric absorption length at the explored densities. The pressure on the ^{4}He sample contained in the cell, about 1 cm^3 in volume, was obtained by direct compression of the room temperature gas, in the range between 3 and 4 kbar, by means of a membrane compressor. The compressed gas is connected to the sample cell through a capillary tube and the pressure is monitored by a strain gauge sensor. Three different thermodynamic paths were followed: (i) the isochore $\rho=37.7$ nm^{-3} for T ranging from 27 K to 210 K; (ii) the isochore $\rho=45.2$ nm^{-3} for T ranging from 27 K to 294 K; (iii) the isotherm $T=27$ K for densities ranging from 30.9 nm^{-3} to 51.4 nm^{-3}. Number densities were calculated using the data in Ref. [7]

Corrections due to the multiple scattering contribution, which depend on the details of the sample shape and the spectrometer optics, were calculated, following a procedure analogous to the one already described in the literature [8], to be less than 2%. Moreover the incoherent contribution to the scattered intensity, originating from a nonspherical symmetry in the electronic charge distribution, can be assumed to be negligible in the case of ^{4}He. The empty cell contribution to the scattered intensity was also found to be negligible. These considerations make us confident that the collected signal is essentially proportional to the convolution of $S(Q,\omega)$ with the experimental resolution function.

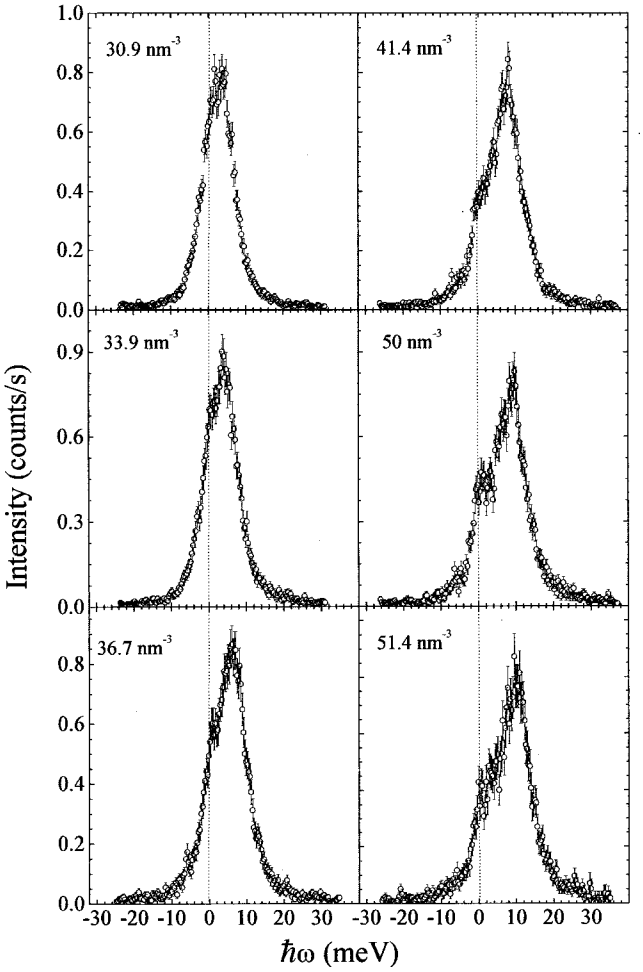

FIG. 1. IXS spectra for exchanged wave vector $Q=7.8$ nm^{-1} from supercritical He at $T=27$ K at different number density values as indicated in the plots. The raw data (open circles), reported in counts per second, are plotted with their error bars; the vertical line marks the zero energy transfer position (elastic scattering).

Examples of IXS spectra measured along the isotherm $T=27$ K and at $Q=7.8$ nm^{-1} are reported in Fig. 1. Two broad and asymmetric shoulders, characteristic of acoustic-like collective excitation, are clearly observable in all the spectra.

III. THEORETICAL BACKGROUND

A. The spectral moments

As already mentioned, the first moment of the dynamic structure factor has the well known exact expression

$$\hbar\langle\omega^1(Q)\rangle=\frac{\hbar^2Q^2}{2M}, \tag{4}$$

which obviously vanishes in the classical limit.

The second spectral moment may be written, following Ref. [10], as (see also Ref. [11])

$$\hbar^2\langle\omega^2(Q)\rangle=\left(\frac{\hbar^2Q^2}{2M}\right)^2[2-S(Q)]+\left(\frac{\hbar^2Q^2}{2M}\right)\times\left[\frac{4}{3}\langle E_{\rm kin}\rangle+K(Q)\right]. \tag{5}$$

Here $\langle E_{\rm kin}\rangle$ denotes the mean (quantum mechanically correct) single particle kinetic energy and

$$K(Q)=\frac{1}{NM}\left\langle\sum_{i\neq j}p_ip_j\cos(\vec{Q}\cdot\vec{r}_{ij})\right\rangle. \tag{6}$$

Obviously in the classical limit one has simply [9]

$$\hbar^2\langle\omega^2(Q)\rangle_C=\frac{\hbar^2Q^2}{2M}\frac{4}{3}\langle E_{\rm kin}\rangle_C=\hbar^2\frac{k_BT}{M}Q^2. \tag{7}$$

It should also be noted that, under the assumption of pairwise additive interatomic potentials, a polynomial $\hbar$ expansion, consistent up to $\hbar^2$ [i.e., up to $\hbar^4$ for $\hbar^2\langle\omega^2(Q)\rangle$], leads to [10]

$$R_2\simeq\left(\frac{\hbar^2Q^2}{2M}\right)+\left[2k_BT+\frac{\hbar^2}{6k_BT}(\Omega_0^2-\Omega_Q^2)\right], \tag{8}$$

where, in terms of the pair distribution function $g(r)$, one has

$$\Omega_Q^2=\frac{\rho}{M}\int g(r)\cos(\vec{Q}\cdot\vec{r})(\hat{Q}\cdot\vec{\nabla})^2U(r)d\vec{r} \tag{9}$$

and

$$\Omega_0^2=\lim_{Q\to0}\Omega_Q^2=\frac{\rho}{M}\int g(r)(\hat{Q}\cdot\vec{\nabla})^2U(r)d\vec{r}, \tag{10}$$

the latter generally being referred to as the square of the Einstein frequency of the fluid.

From these formulas it is readily seen that, in the leading terms of the $\hbar$ expansion R_2 tends to a finite value $2k_BT$, namely, to the ratio of the classical second moment to the exact first moment, in the limit of both low Q and high T; we will refer to this limit as the classical approximation to R_2. Finally, since the third spectral moment, under the assumption of pairwise additive interatomic potentials, is easily derived [12], we can derive an exact expression for R_3 which reads

$$R_3=\left(\frac{\hbar^2Q^2}{2M}\right)^2+4\left(\frac{\hbar^2Q^2}{2M}\right)\langle E_{\rm kin}\rangle+\hbar^2(\Omega_0^2-\Omega_Q^2). \tag{11}$$

Thus in principle if the pair distribution function and the intermolecular potential are known the measurement of R_3 provides the value of $\langle E_{\rm kin}\rangle$.

B. The model line shape

The model line shape adopted is a modification of the line shape obtained from the classical viscoelastic theory of liquids [13], which can be rewritten as

$$S_C(Q,\omega)=A\frac{\tau(\omega_\infty^2-\omega_0^2)}{[\tau\omega(\omega^2-\omega_\infty^2)]^2+(\omega^2-\omega_0^2)^2}, \tag{12}$$

where A, τ, ω_0^2, and ω_∞^2 are four Q dependent parameters representing the intensity, the generalized Maxwell relaxation time, and the infinite and zero frequency limits of the generalized sound dispersion modes, respectively. These last two parameters are related to the first two even nondiverging spectral moments of $S_C(Q,\omega)$. The modification is performed in order to reproduce the quantum character of the spectral line shape, which owing to detailed balance exhibits an evident asymmetry (see Fig. 1). This asymmetry was recovered by multiplying the classical symmetrical line shape by a temperature dependent factor to yield

$$S_M(Q,\omega)=\frac{\hbar\omega}{k_BT}[n(\omega)+1]S_C(Q,\omega), \tag{13}$$

where $n(\omega)$ is the usual Bose-Einstein population factor. This procedure, which is in a sense rigorous only for the harmonic oscillator, obviously alters the spectral moments of the classical line shape, introducing nonvanishing odd spectral moments and rendering the fourth moment divergent. In the following we shall treat this a line shape as a model line shape with four entirely free parameters which turns out to be sufficiently flexible to reproduce our data at all investigated Q values, yielding finite spectral moments up to order 3.

IV. DATA ANALYSIS

The fitting procedure was performed using a χ^2 minimization of the line shape previously described, accounting for the experimentally measured instrumental resolution function $R(\omega)$ and allowing for a constant background B. In practice the adopted fitting line shape is given by

$$f(q,\omega)=R(\omega)\otimes S_M(Q,\omega)+B, \tag{14}$$

where $\otimes$ stands for a convolution integral which is performed numerically. During the fitting procedure, as already stressed, ω_∞^2, ω_0^2, A, and τ are all left free to vary without any constraint on their Q dependence. Figure 2(a) shows a typical IXS raw spectrum (open circles) at a density of 51.4 nm^{-3}, 27 K, and $Q=7.8$ nm^{-1}, together with the corresponding best fit line shape. The two are also reported on a logarithmic scale in the inset to better illustrate the agreement between experimental and best fit line shapes even in the tails. The vertical arrow indicates the zero energy transfer (elastic scattering) position.

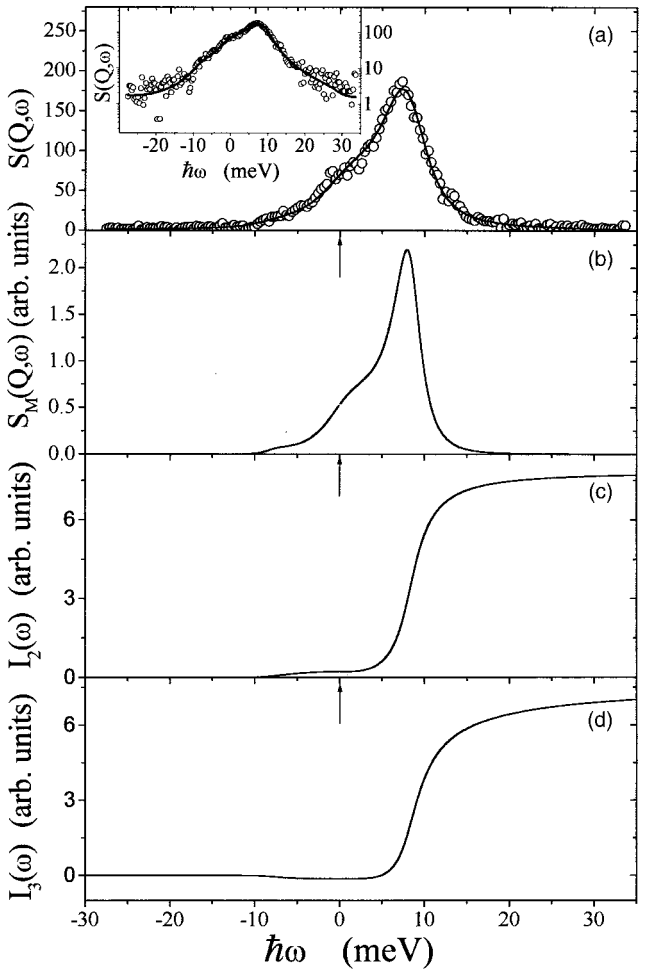

FIG. 2. (a) An IXS spectrum and its best fit line shape with model (12) at $\rho=51.4$ nm^{-3}, 27 K, and $Q=7.8$ nm^{-1} (total number of counts is reported); the same is reported on a logarithmic scale in the inset. (b) The best fit model (resolution free) line shape $S_M(Q,\omega)$ of the same spectrum, obtained from Eq. (13). (c) and (d) The cumulative integrals $I_2(\omega)$ and $I_3(\omega)$ of Eq. (15) in arbitrary units as functions of the upper integration limit. The vertical arrows mark the zero energy transfer position.

Figure 2(b) shows the corresponding resolution free spectral densities $S_M(Q,\omega)$ obtained from the best fit parameters, while Figs. 2(c) and 2(d) show the cumulative integrals of the second and third spectral moments given, respectively, by

$$I_2(\omega)=\hbar^2\int_{-\infty}^{\omega}\omega'^2 S_M(Q,\omega')d\omega',$$

$$I_3(\omega)=\hbar^3\int_{-\infty}^{\omega}\omega'^3 S_M(Q,\omega')d\omega', \qquad (15)$$

which have been calculated for every fitted spectrum in order to check for the convergence of the spectral moment within the fitted spectral region.

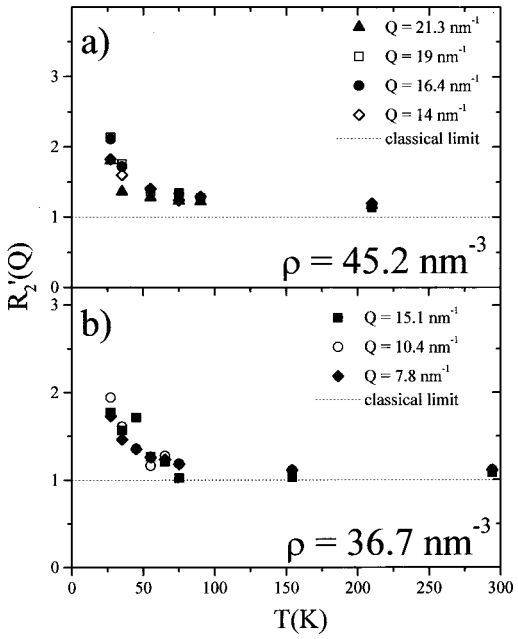

FIG. 3. The reduced value of R_2, $R_2'=(R_2-\hbar^2Q^2/2M)(2k_BT)^{-1}$, as measured for the selected Q and density values indicated in the plots.

V. DISCUSSION

Reduced values of R_2', obtained from R_2 after subtracting the recoil term $\hbar^2Q^2/2M$ and normalizing to the classical value $2k_BT$, are reported as a function of temperature in Figs. 3(a) and 3(b) along the two isochores at $\rho=45.2$ nm^{-3} and 36.7 nm^{-3}, respectively. From the two plots we see that (i) the classical limit is reached, at temperatures well below the highest investigated temperature, for both densities, although the approach to this limit seems to be faster the lower the density; (ii) at lower temperatures, where quantum deviation become relevant, an increasing Q spread of the data is observed, indicating larger quantum effects with increasing Q. This temperature behavior is not surprising as the amplitude of quantum effects is expected to vary roughly as the ratio between the de Broglie wavelength and the mean interparticle distance, namely, as $T\rho^{-1/3}$.

In Fig. 4 we report the density dependence of the reduced R_2' for five Q values (namely, 7.8,10.4,12.7,15.1, and 17.6 nm^{-1}) at the lowest investigated temperature $T=27$ K. It can be seen that the curves at different Q values tend to diverge as the density increases, consistently with the expected density increase of $(\Omega_0^2-\Omega_Q^2)$. The dotted horizontal line represents the classical limit, which has to be reached in the low-density (perfect gas) and/or low-Q (macroscopic) limits at least in the leading terms of the $\hbar$ expansion.

The Q dependence of the reduced R_2' extending from 2.5 nm^{-1} to 26.5 nm^{-1} is shown in Fig. 5 for the two extreme investigated temperatures ($T=27$ K and 294 K, respectively) along the isochore at $\rho=36.7$ nm^{-3} The different role of the quantum effects at the two temperatures is quite remarkable.

It should be noted that since

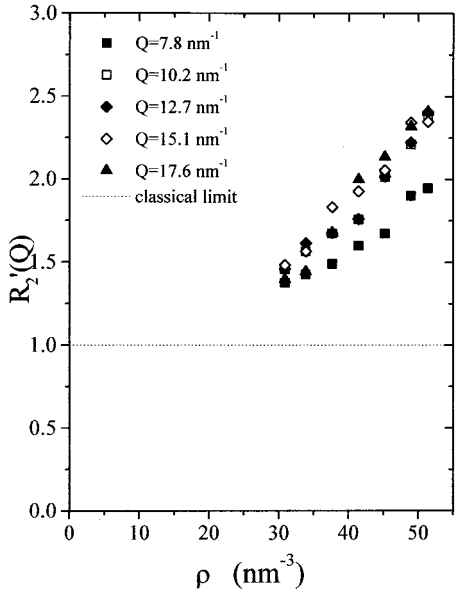

FIG. 4. The same quantity as in Fig. 3 but reported as a function of density along the isotherm $T=27$ K.

$$\lim_{Q\to\infty} R_2(Q)=\frac{\hbar^2Q^2}{2M}+\frac{4}{3}\langle E_{\rm kin}\rangle, \tag{16}$$

a study of the Q dependence of $R_2(Q)$, once extended to sufficiently high Q values, can provide a straightforward measurement of the quantum effects on $\langle E_{\rm kin}\rangle$. This is usually exploited in neutron Compton scattering experiments [1,2] where the single particle scattering regime is almost reached. Unfortunately this limit is far from being reached

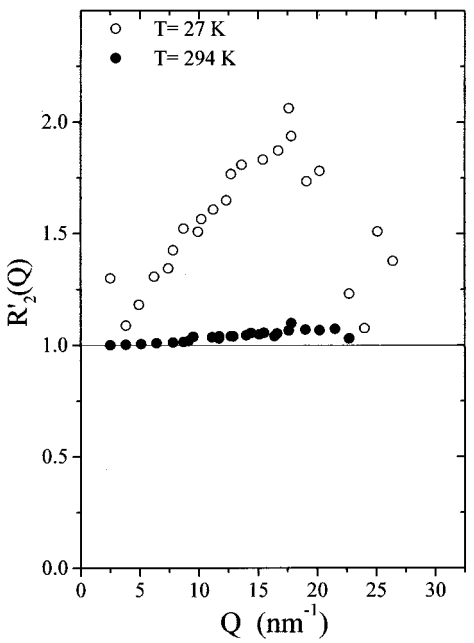

FIG. 5. The same quantity as in Figs. 3 and 4 reported as a function of the exchanged momentum at a density $\rho=36.7$ nm^{-3} for the two extreme temperatures 27 K (full circles) and 294 K (open circles).

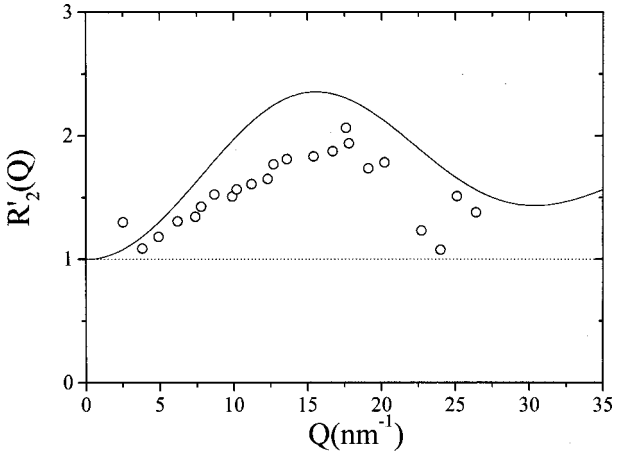

FIG. 6. Comparison between the experimental value of the reduced second moment R_2' (open circles) and the truncated $\hbar$ expansion of Eq. (8), computed as discussed in the text (solid line), at $\rho=36.7$ nm^{-3} and $T=27$ K.

even at the highest Q values explored in the present experiment; therefore we looked for an alternative strategy.

As a preliminary step we evaluated the $\hbar$ expansion approximation of Eq. (8) to the second moment by numerically calculating the quantity $(\Omega_0^2-\Omega_Q^2)$, making use of the Aziz potential [14] and available $g(r)$'s at $T=20$ K and $\rho=33$ nm^{-3} [15] obtained from neutron diffraction measurements. The comparison between our IXS data for R_2' at $\rho=36.7$ nm^{-3} and $T=27$ K and these calculations is reported in Fig. 6. The agreement is only qualitative and the observed discrepancies would lead us to believe that, while at these thermodynamic conditions the truncated $\hbar$ expansion seems adequate for low Q values, it is definitely not so at larger Q values. In order to accept this conclusion one must be confident that the data analysis procedure based on the model line shape described yields reliable spectral moment values.

In order to check the reliability of our spectral moments we compared the values obtained for R_3 at the same thermodynamic points with the predictions of Eq. (11). In this case exact values can be predicted if the single particle kinetic energy $\langle E_{\rm kin}\rangle$ is known. This was obtained by interpolating the (ρ,T) contour plot of the kinetic energy obtained from the path integral Monte Carlo (PIMC) calculations reported in Ref. [4]. The comparison is reported in Fig. 7, where we show also the R_3 values obtained using the classical value $\frac{3}{2}k_BT$ for the kinetic energy. Despite some scattering of the data, particularly around Q_m, the agreement between predicted and measured values is rather good when the quantum values of $\langle E_{\rm kin}\rangle$ are used. This finding makes us confident of the reliability of the experimentally determined R_3 values, thus *a posteriori* validating also the experimental determination of R_2 already discussed.

A further consequence is that, provided $(\Omega_0^2-\Omega_Q^2)$ is known, Eq. (11) can be inverted to obtain a direct measure of $\langle E_{\rm kin}\rangle$ also at finite Q values,

$$\langle E_{\rm kin}\rangle=\frac{1}{4}\left(\frac{R_3(Q)-\hbar^2(\Omega_0^2-\Omega_Q^2)}{\hbar^2Q^2/2M}-\frac{\hbar^2Q^2}{2M}\right). \tag{17}$$

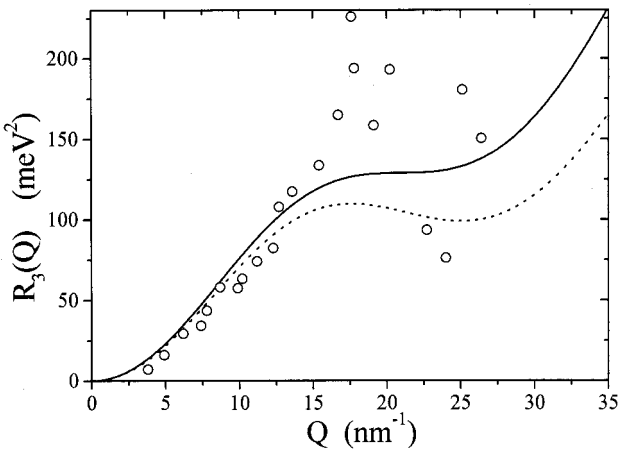

FIG. 7. Comparison between the experimental value of the third moment ratio R_3 (open circles) and its theoretical prediction given by Eq. (11), as discussed in the text (lines). The two lines correspond to different guesses for the kinetic energy $\langle E_{\rm kin}\rangle$: (i) the classically expected value $3k_BT/2$ (dashed line); (ii) an estimation by interpolating kinetic energy PIMC (ρ,T) contour plots [4] (solid line).

In our case the kinetic energies $\langle E_{\rm kin}\rangle$ obtained for all the available Q values, albeit quite scattered, yield an average value of 63 K with a statistical uncertainty of ± 10 K, in fair agreement with the value of 70 K interpolated from PIMC results [4].

A detailed discussion of the analysis of the spectra in terns of the viscoelastic model and of the physical interpretation of the fit parameters will be reported in a further study.

VI. CONCLUSIONS

We have proposed an experimental method to characterize quantum deviations of the dynamics of supercritical helium. Its dynamic structure factor $S(Q,\omega)$ has been measured as a function of both T and ρ and in an intermediate dynamic range, i.e., at Q values below and around the first diffraction maximum and with ω ranging in the THz region. Quantum effects have been studied by looking at their signatures in the first three spectral moments of experimental spectra. As expected the weight of the quantum deviations has been found to grow systematically when the temperature is lowered and when the exchanged momentum and/or the density are increased.

In particular, as far as the third moments are concerned, we have found the Q behavior to be fairly well approximated by a formula valid for a pairwise additive potential in which experimentally determined neutron diffraction pair distribution functions and the Aziz interparticle potential are used together with previous PIMC computations for the single particle kinetic energy $\langle E_{\rm kin}\rangle$. Moreover, we have shown that a value of $\langle E_{\rm kin}\rangle$ that is consistent with the PIMC predictions can be extracted with our data analysis even from a dynamic region where collective modes are still dominats. Efforts are in progress to extend this study, in order to obtain measurements of $\langle E_{\rm kin}\rangle$ along the whole dynamic region between the hydrodynamic and single particle regimes.

[1] C. Andreani, A. Filabozzi, M. Nardone, F. P. Ricci, and J. Mayers, Phys. Rev. B **50**, 12 744 (1994); F. Albergamo, M. Nardone, and A. Filabozzi, *ibid.* **56**, 14 614 (1997).

[2] U. Bafile, M. Zoppi, F. Barocchi, R. Magli, and J. Mayers, Phys. Rev. Lett. **75**, 1957 (1995); R. T. Azuah, W. G. Stirling, H. R. Glyde, M. Boninsegni, P. E. Sokol, and S. M. Bennington, Phys. Rev. B **56**, 14 620 (1997).

[3] D. M. Ceperley and E. L. Pollock, Phys. Rev. Lett. **56**, 351 (1986); R. C. Blasdell, D. M. Ceperley, and R. O. Simmons, Z. Naturforsch., A: Phys. Sci. **48A**, 433 (1993).

[4] D. M. Ceperley, R. O. Simmons, and R. C. Blasdell, Phys. Rev. Lett. **77**, 115 (1996).

[5] V. F. Sears, Phys. Rev. B **30**, 44 (1984); H. R. Glyde, *ibid.* **50**, 6726 (1994); S. Stringari, *ibid.* **35**, 2038 (1987); for a comprehensive overview of the different theoretical approaches, see *Moment Distribution*, edited by H. R. Silver and P. E. Sokol (Plenum, New York, 1989), and references therein.

[6] C. Masciovecchio *et al.*, Nucl. Instrum. Methods Phys. Res. B **111**, 181 (1996).

[7] V. V. Sychev, A. A.Vasserman, A. D. Kozlov, G. A. Spiridonov, and V. A. Tsymarny, *Thermodynamic Properties of Helium* (Hemisphere Publishing Corporation, Washington, DC, 1987).

[8] G. Monaco, A. Cunsolo, G. Ruocco, and F. Sette, Phys. Rev. E **60**, 5505 (1999).

[9] U. Balucani, and M. Zoppi, *Dynamics of the Liquid State* (Clarendon Press, Oxford, 1994).

[10] H. Fredrikze, Mol. Phys. **48**, 903 (1983).

[11] S. Stringari, Phys. Rev. B **46**, 2974 (1992).

[12] R. D. Puff, Phys. Rev. **137**, A406 (1965).

[13] S. W. Lovesey, J. Phys. C **4**, 3057 (1971).

[14] R. W. Aziz, V. P. S. Nain, J. S. Carley, W. L. Taylor, and G. T. McConville, J. Chem. Phys. **70**, 4330 (1979).

[15] F. Albergamo, A. Filabozzi, and M. Nardone (unpublished).